The catalytic activity of the highly dispersed solid solution $Ce_{0.80}Zr_{0.10}La_{0.05}M_{0.05}O_{2-\delta}$ (where *M* = Nd, Sm or Gd) in the complete oxidation reaction of methane

E. Yu. Liberman, *Doctor of Chemical Sciences, Professor, Department of Technology of Inorganic Substances and Electrochemical Processes*[1], *e-mail: liberman.e.i@muctr.ru*
T. V. Kon'kova, *Doctor of Technical Sciences, Professor, Department of Technology of Inorganic Substances and Electrochemical Processes*[1], *e-mail: konkova.t.v@muctr.ru*
A. M. Gaidukova, *Candidate of Technical Sciences, Associate Professor, Department of Technology of Inorganic Substances and Electrochemical Processes*[1], *e-mail: gaydukovaAM@yandex.ru*
I. V. Zagaynov, *Candidate of Chemical Sciences, Senior Researcher, Laboratory of Functional Ceramics, Laboratory of Functional Ceramics*[2], *e-mail: igorscience@gmail.com*

[1]*Mendeleev University of Chemical Technology, Moscow, Russia.*
[2]*A. A. Baikov Institute of Metallurgy and Materials Science of the Russian Academy of Sciences, Moscow, Russia.*

Highly dispersed, fluorite-like solid solutions ($Ce_{0.80}Zr_{0.10}La_{0.05}M_{0.05}O_{2-\delta}$), where *M* = Nd, Sm or Gd, were synthesized by co-precipitating metal hydroxides, followed by heat treatment. The chemical composition of the resulting materials was confirmed by inductively coupled plasma optical emission spectroscopy. *X*-ray phase analysis confirmed the formation of the $Ce_{0.80}Zr_{0.10}La_{0.05}M_{0.05}O_{2-\delta}$ solid solutions, where *M* = Nd, Sm or Gd, based on the cerium dioxide crystal lattice. According to transmission electron microscopy data, the average particle size is 13 ± 2 nm. The synthesised materials have a mesoporous structure with a specific surface area of 83–86 m^2/g, a total pore volume of 0.101–0.104 cm^3/g and a pore diameter of 3.6–3.8 nm. The catalysts exhibit high activity in the complete oxidation of methane (model mixture composition: CH_4 – 1 vol.%; O_2 – 8 vol.%; N_2 – balance). A correlation has been established between the catalytic activity of solid solutions and the ionic radius of the rare earth dopant *M*. The activity of synthesised solid solutions ($Ce_{0.80}Zr_{0.10}La_{0.05}M_{0.05}O_{2-\delta}$), where *M* = Nd, Sm or Gd, decreases in the order Gd → Sm → Nd. The highest activity is observed in the presence of the $Ce_{0.80}Zr_{0.10}La_{0.05}M_{0.05}O_{2-\delta}$ catalyst, which has the smallest ionic radius of the M^{3+} dopants studied. The temperatures at which 50% and 99% conversion are achieved in the presence of the sample are 356 °C and 477 °C, respectively. The application of $Ce_{0.80}Zr_{0.10}La_{0.05}M_{0.05}O_{2-\delta}$ as a carrier for the active component, palladium, shows promise. The catalytic activity of 0.3% $PdO/Ce_{0.80}Zr_{0.10}La_{0.05}M_{0.05}O_{2-\delta}$ exceeds that of the industrial analogue, 0.3% $PdO/\gamma\text{-}Al_2O_3$, demonstrating the feasibility of using the synthesized solid solution as a carrier for the active component.

Key words: cerium dioxide, solid solution, complete oxidation of methane, catalytic oxidation of methane.
DOI: 10.17580/nfm.2025.02.05

Introduction

One of the trends in the development of the modern economy is the transition to low-carbon energy. This involves using methane not only as an energy source, but also as a raw material for chemicals. The most significant industrial method of methane processing currently is the production of synthesis gas ($CO + H_2$), the basis for synthesising ammonia, methanol, acetic acid and synthetic gasoline. Of particular interest is the use of methane as a reducing agent in metallurgy for the direct reduction of iron ore in the form of metallised pellets (DRI, or Direct Reduced Iron) and hot briquetted iron (HBI), which reduces energy consumption and gas emissions compared to the traditional process [1]. However, methane has a significant disadvantage in that its greenhouse effect is 10–12 times greater than that of carbon dioxide, so it is necessary to prevent it from entering the atmosphere [2]. Additionally, the temperature rises to 1400 °C during the oxidation of methane due to the exothermic nature of the reaction. This results in the formation of NO_x, as well as incomplete combustion products such as: CO and soot. One solution is to purify gas emissions through catalytic (flameless) methane combustion [3, 4]. The complete oxidation of methane is a catalytic reaction that occurs at temperatures below 600 °C. This prevents CO and soot from entering the atmosphere and reduces the NO_x content to 5 ppm. In contrast, non-catalytic oxidation produces 150–200 ppm of NO_x [4]. Catalysts based on noble metals ($MO_x/\gamma\text{-}Al_2O_3$, where *M* is Pd or Pt) are typically used for the complete catalytic oxidation of methane. Their advantages are their high

activity and low cost, while their disadvantages are their low thermal stability. This problem could be solved by using complex oxide compositions based on *d*- and *f*-element oxides, such as perovskites and ferrites [3]. Cerium-containing fluorite-like solid solutions are promising as they can be used as both catalysts and carriers of active components. Unlike γ-Al_2O_3, these components exhibit their own activity, which increases the catalyst's service life and reduces the process temperature [3–7].

This study aimed to investigate the catalytic activity of highly dispersed multicomponent solid solutions ($Ce_{0.80}Zr_{0.10}La_{0.05}M_{0.05}O_{2-\delta}$), where M = Nd, Sm or Gd, in the complete oxidation reaction of methane. The study also examined the potential use of these materials as carriers for the active component, PdO, and compared the synthesised materials with the industrial analogue, 0.3% PdO/γ-Al_2O_3.

Experimental part

The synthesis of $Ce_{0.80}Zr_{0.10}La_{0.05}M_{0.05}O_{2-\delta}$, where M is either Nd, Sm or Gd, was carried out by co-precipitation of cerium, zirconium, and rare earth metal hydroxides. Rare earth metal nitrates were used for the synthesis: $Ce(NO_3)_3$ (p.a.), $La(NO_3)_3$ (p.a.), $Nd(NO_3)_3$ (p.a.), $Sm(NO_3)_3$ (p.a.), $Gd(NO_3)_3$ (p.a.), and $ZrO(NO_3)_2$ (p.a.). Isopropyl alcohol was used to prepare the initial metal nitrate solutions. The concentration of the metal nitrate solutions was 0.5 mol/L. The salt solutions were then mixed in a stoichiometric ratio of Ce : Zr : La : M = 16 : 2 : 1 : 1, which corresponds to the chemical composition of the solid solution $Ce_{0.80}Zr_{0.10}La_{0.05}M_{0.05}O_{2-\delta}$. Precipitation was carried out by adding ammonia solution (0.5 mol/L) (puriss. spec.) until a pH of 10–11 was reached. The precipitate was kept under a layer of the mother liquor for 1 hour, then filtered on a vacuum filter and thoroughly washed with distilled water. The precipitate was dried at 95 °C for 10 hours in a drying oven and calcined in a muffle furnace at 600 °C for 2 hours, with a temperature rise rate of 5 °C/min.

The calculated amount of the palladium acetylacetonate precursor ($Pd(C_2H_7O_2)_2$), at a concentration of 0.3 wt.% (based on the metal content), was dissolved by heating in ethanol. This solution was then mixed with the synthesised sample and held at the boiling point of ethanol (78 °C) until the solvent had completely evaporated. The solution was then calcined at 350 °C for two hours with a temperature rise rate of 5 °C/min.

For the comparative study, an analogue of the industrial catalyst, 0.3% PdO/Al_2O_3, was prepared using granulated γ-Al_2O_3 (AOK-63-11, grade B, granule size 0.4 – 1 mm, specific surface area 185 m^2/g and total pore volume 0.501 cm^3/g) as a carrier. The PdO was applied using the above-described method.

The phase composition of the synthesised materials was studied using *X*-ray diffraction with a Bruker D8 Advance (Bruker) instrument with monochromatic CuK_α radiation (λ = 1.5418 Å), with a step size of 0.01° and an accumulation time of 0.3 s/step. The crystallographic characteristics were calculated using full-profile analysis with Topas R software. The coherent scattering region (CSR) was calculated using the Selakov-Sherrer equation.

The elemental composition of the samples was determined using inductively coupled plasma optical emission spectroscopy (ICP-OES) on an Agilent 5800 VDV ICP-OES spectrometer (Agilent Technologies).

Transmission electron microscopy (TEM) was used to determine particle size. The studies were conducted using a JEOL JEM-2100 electron microscope (resolution – 0.18 nm, voltage – 200 kV). To eliminate particle agglomeration, preliminary dispersion in isopropyl alcohol was performed. The resulting suspensions were sonicated for 10 minutes in an ultrasonic disperser. Then, 10 µl of the sample suspension was taken and applied to a special copper mesh with an amorphous carbon film.

The textural characteristics of the synthesized samples were studied by low-temperature nitrogen adsorption on a NOVA 1200e analyzer (Quantachrome). The samples were activated at 200 °C for 4 hours. The specific surface area of the materials (S_{sp}) was calculated using the Brunauer-Emmett-Teller (BET) equation in the P/P_s range from 0.05 to 0.3. The total pore volume (V_Σ) was determined at a relative pressure of P/P_s 0.99. The volume of micropores was calculated using the t-method with the installation software. The average pore diameter was calculated using the formula:

$$D = \frac{4V}{S_{sp}}. \quad (1)$$

The catalytic activity of the synthesised materials in the complete oxidation reaction of methane was determined using the flow method. One gram of the catalyst was mixed with quartz to prevent localised overheating, then placed in a *U*-shaped quartz reactor. A gas mixture was then passed through the reactor and heated to the required temperature. The catalysts were tested for complete methane conversion using a model mixture of: CH_4 – 1 vol.%; O_2 – 8 vol.%; N_2 – balance (Linde Gas Russia OJSC), with a flow rate of 60 ml/min and a temperature range of 20–700 °C. The concentrations of the gas mixture components (O_2, N_2, CO, CH_4, CO_2 and H_2O) were determined using a CHROM-5 gas chromatograph (CHROM). NaX (l = 2.5 m, d = 3 mm) and PoraPak Q (l = 5 m, d = 2 mm) molecular sieve columns were used for separation. A thermal conductivity detector was used to record the signal. The chromatograms were processed using Ekokhrom software.

To calculate the conversion of methane X, the following equation was used:

$$X = \frac{c_o - c}{c_o}, \quad (2)$$

where C_0 is the methane concentration in the initial gas mixture (vol.%), C is the methane concentration in the mixture at the reactor outlet (vol.%).

To evaluate the activity of the catalysts, the temperatures at 50% and 99% methane conversion were used.

Results and discussion

Fig. 1 shows the results of the *X*-ray diffraction study of the phase composition of the synthesized materials.

Reflections 28.5; 33.1; 47.5; 56.3; 59.1; 69.4; 76.7 and 79.1 correspond to the crystallographic planes (111), (200), (220), (311), (222), (400), (331), and (420) of the cubic lattice of cerium dioxide (JSPDS No. 81-0792). No peaks attributable to zirconium or rare earth metal compounds were observed in the *X*-ray diffractograms. However, the molar ratio of the components of the synthesized samples corresponds to the conditions specified in the experiment, as determined by elemental analysis. It appears that the single-phase composition of the samples is due to the formation of solid substitution solutions based on the cubic lattice of cerium dioxide [8, 9]. At the same time, the lattice parameter of the synthesized compositions differs slightly from that of cerium dioxide.

According to the residual crystal size (RCS) calculation results for the synthesised samples, carried out using the Selakov-Sherrer equation, the size of the crystallites in the solid solutions is smaller than that of cerium dioxide (25.2 nm). This is due to the dopants partially segregating on the surface, which increases the system's dispersion [10]. Reflections characteristic of palladium compounds could not be detected on the *X*-ray diffractogram of 0.3% $PdO/Ce_{0.85}Zr_{0.15}La_{0.05}O_{2-\delta}$ due to insufficient content for identification by *X*-ray diffraction.

According to the results of studies conducted using the TEM method, the synthesized materials have an agglomerated mosaic-type structure. The particles are spherical in shape, with an average size of 13 ± 2 nm. At the same time, particles of the deposited palladium-containing compounds are not visualized on the surface of the $PdO/Ce_{0.80}Zr_{0.10}La_{0.05}Gd_{0.05}O_{2-\delta}$ sample, particles of deposited palladium-containing compounds are not visualized, which may be due to both the high density of cerium-containing materials, which makes research difficult, and the possible formation of surface nanostructures that cannot be detected by TEM (**Fig. 2**) [11].

The synthesized solid solutions belong to mesoporous structures, as evidenced by the presence of capillary-condensation hysteresis on nitrogen adsorption-desorption isotherms (**Fig. 3**). Nitrogen adsorption-desorption isotherms belong to type IV isotherms according to the IUPAC nomenclature. According to de Boer's classification, the hysteresis loop shape corresponds to H_2, characteristic of materials with a corpuscular structure having a heterogeneous distribution of pores by size [12]. The average pore diameter of the synthesized materials is 4.5–5.0 nm **(Table)**. Doping cerium dioxide with Zr^{+4}, La^{+3}, Nd^{+3}, and Gd^{+3} ions is accompanied by an increase in specific surface area from 56 m^2/g to 83–86 m^2/g and an increase in pore volume from 0.063 to 0.107 cm^3/g, respectively. Apparently, the reason for this is the formation

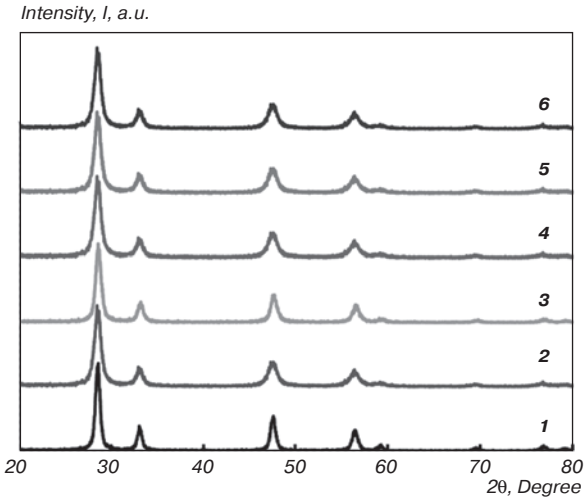

Fig. 1. *X*-ray diffraction pattern of synthesized samples:
1 – CeO_2; *2* – $Ce_{0.80}Zr_{0.10}La_{0.10}O_{2-\delta}$;
3 – $Ce_{0.80}Zr_{0.10}La_{0.05}Nd_{0.05}O_{2-\delta}$;
4 – $Ce_{0.80}Zr_{0.10}La_{0.05}Sm_{0.05}O_{2-\delta}$;
5 – $Ce_{0.80}Zr_{0.10}La_{0.05}Gd_{0.05}O_{2-\delta}$;
6 – $PdO/Ce_{0.80}Zr_{0.10}La_{0.05}Gd_{0.05}O_{2-\delta}$

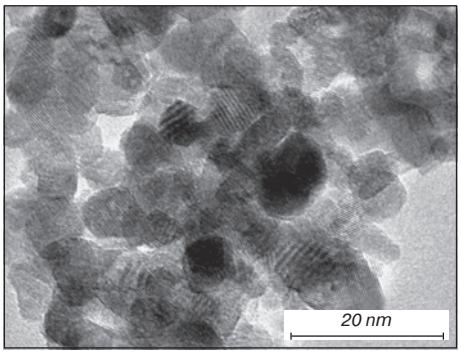

Fig. 2. Transmission electron microscopy micrograph of the sample $0.3\%PdO/Ce_{0.85}Zr_{0.15}La_{0.05}O_{2-\delta}$

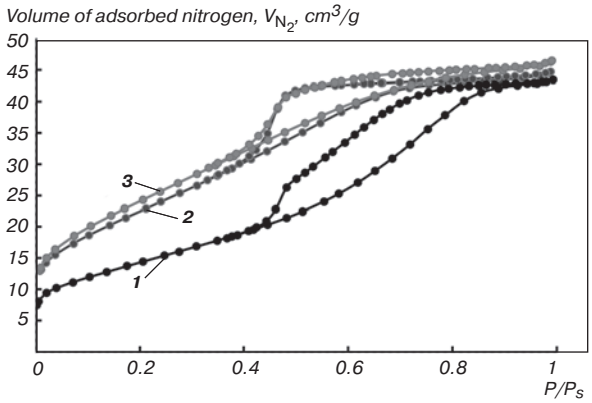

Fig. 3. Isotherm of nitrogen adsorption-desorption of synthesized samples:
1 – CeO_2; *2* – $PdO/Ce_{0.80}Zr_{0.10}La_{0.05}Gd_{0.05}O_{2-\delta}$;
3 – $Ce_{0.80}Zr_{0.10}La_{0.05}Gd_{0.05}O_{2-\delta}$

of solid solutions accompanied by a restructuring of the crystal structure, leading to the development of the surface and an increase in defectivity. After palladium impregnation on the surface of $Ce_{0.85}Zr_{0.15}La_{0.05}O_{2-\delta}$, a slight

Table
Crystallographic characteristics, textural properties, and catalytic activity of synthesized samples

Chemical composition of the sample	Crystallographic characteristic		Textural characteristics				Catalytic activity	
	a, Å	RCS, nm	S_{sp}, m^2/g	V^*_{mi}, cm^3/g	V_{Σ}, cm^3/g	D, nm	$T_{50\%}$, °C	$T_{99\%}$, °C
CeO_2	5.423	25.2	56	0.02	0.083	4.5	495	645
$Ce_{0.80}Zr_{0.10}La_{0.10}O_{2-\delta}$	5.416	16.9	82	0.03	0.101	4.9	472	606
$Ce_{0.80}Zr_{0.10}La_{0.05}Nd_{0.05}O_{2-\delta}$	5.413	16.7	86	0.04	0.107	5.0	441	575
$Ce_{0.80}Zr_{0.10}La_{0.05}Sm_{0,05}O_{2-\delta}$	5.414	15.9	85	0.04	0.103	4.8	408	516
$Ce_{0.80}Zr_{0.10}La_{0.05}Gd_{0.05}O_{2-\delta}$	5.411	15.4	83	0.04	0.104	5.0	356	477
$PdO/Ce_{0.80}Zr_{0.10}La_{0.05}Gd_{0.05}O_{2-\delta}$	5.415	16.5	81	0.04	0.090	4.4	285	395
*micropores								

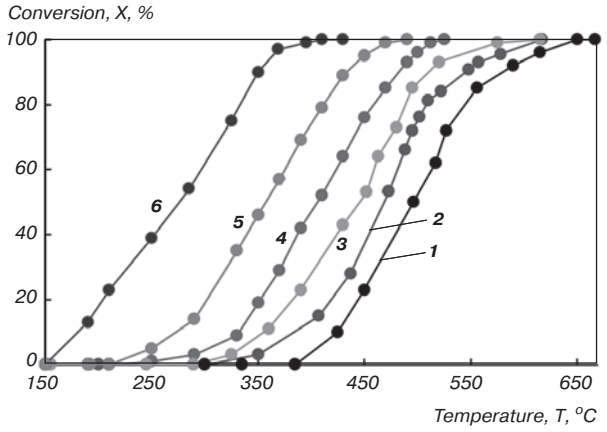

Fig. 4. Catalytic activity of synthesized samples in the complete oxidation of methane reaction:
1 – CeO_2, *2* – $Ce_{0.80}Zr_{0.10}La_{0.10}O_{2-\delta}$,
3 – $Ce_{0.80}Zr_{0.10}La_{0.05}Nd_{0.05}O_{2-\delta}$,
4 – $Ce_{0.80}Zr_{0.10}La_{0.05}Sm_{0.05}O_{2-\delta}$,
5 – $Ce_{0.80}Zr_{0.10}La_{0.05}Gd_{0.05}O_{2-\delta}$,
6 – $PdO/Ce_{0.80}Zr_{0.10}La_{0.05}Gd_{0.05}O_{2-\delta}$

decrease in specific surface area and porosity is observed, which is associated with partial pore overlap **(Table)**.

A comparative analysis of methane conversion curves 1–4 (**Fig. 4**) demonstrates the advantage of multicomponent systems over cerium dioxide, which is due to the formation of Se^{+3} ions, anionic vacancies, and crystallographic distortions resulting from lattice rearrangement as a result of heterovalent doping. Thus, the temperatures of 50% and 99% conversion in the presence of the $Ce_{0.80}Zr_{0.10}La_{0.05}Gd_{0.05}O_{2-\delta}$ sample are 356 °C and 477 °C, respectively, while for CeO_2 they are 495 °C and 645 °C, respectively.

The observed difference in the activity of the synthesized samples can be interpreted as follows. One of the stages of catalytic oxidation of methane on oxide catalysts is the adsorption of molecular oxygen on the surface. It is known that the presence of anionic vacancies increases the adsorption capacity of molecular oxygen on the catalyst surface, which leads to an increase in catalytic activity [9]. Solid solutions obtained by heterovalent doping have a large number of anion vacancies compared to cerium dioxide, which is the reason for the higher catalytic activity of the samples.

Lattice oxygen, i.e., oxygen that is part of the crystal lattice, also participates in the oxidation of methane on cerium-containing catalysts. Its mobility is largely determined by the strength of the metal-oxygen bond. Apparently, as a result of the formation of solid solutions due to crystallographic distortions and the appearance of anion vacancies, structures are formed in which the metal-oxygen bond energy is lower than that of cerium dioxide, which contributes to higher catalytic activity.

It should also be noted that the presence of Ce^{3+} ions contributes to increased activity due to the presence of the Ce^{3+}/Ce^{4+} redox transition, which participates in the oxidation of adsorbed molecular oxygen and the transport of lattice oxygen.

For the samples studied, catalytic activity decreases in the following order:

$Ce_{0.80}Zr_{0.10}La_{0.05}Gd_{0.05}O_{2-\delta} >$
$> Ce_{0.80}Zr_{0.10}La_{0.05}Sm_{0.05}O_{2-\delta} >$
$> Ce_{0.80}Zr_{0.10}La_{0.05}Nd_{0.05}O_{2-\delta}$.

Apparently, the observed effect is due to the formation of a crystal structure that provides higher mobility of lattice oxygen.

At the same time, there is a correlation between the temperature of 99% oxidation of cerium-containing solid solutions and the ionic radius of dopant M. Thus, the catalytic activity of the synthesized samples increases with a decrease in the ionic radius of dopant M. It should be noted that similar results were obtained by the authors when studying the catalytic activity of cerium-containing solid solutions in CO oxidation reactions [13].

The $Ce_{0.85}Zr_{0.15}La_{0.05}O_{2-\delta}$ sample was selected as the carrier for the active component – palladium oxide (PdO) – which exhibits high activity in oxidative catalysis processes due to the Pd^{2+}/Pd^{4+} redox transition. The 0.3% $PdO/Ce_{0.85}Zr_{0.10}La_{0.05}O_{2-\delta}$ catalyst exhibited higher catalytic activity in comparison to the 0.3% PdO/Al_2O_3 reference sample. The observed effect is attributable not

only to the manifestation of the $Ce_{0.85}Zr_{0.10}La_{0.05}O_{2-\delta}$ carrier's inherent catalytic activity, but also to the enhanced dispersibility of the deposited component on the carrier surface, resulting in the formation of smaller palladium oxide particles, which contributes to an increase in catalytic activity. [14].

Conclusion

Based on the studies conducted, it can be concluded that highly dispersed, fluorite-like solid solutions of the form $Ce_{0.80}Zr_{0.10}La_{0.05}M_{0.05}O_{2-\delta}$, where M = Nd, Sm or Gd, exhibit high catalytic activity in the complete oxidation reaction of methane. A correlation has been established between catalytic activity and the ionic radius of the rare earth dopant. The most active sample is $Ce_{0.80}Zr_{0.10}La_{0.05}Gd_{0.05}O_{2-\delta}$, due to the formation of a structure with greater crystallographic distortion compared to Nd^{3+} and Sm^{3+} ions. The $Ce_{0.80}Zr_{0.10}La_{0.05}Gd_{0.05}O_{2-\delta}$ solid solution can be used as a carrier, with the $PdO/Ce_{0.80}Zr_{0.10}La_{0.05}Gd_{0.05}O_{2-\delta}$ activity exceeding that of PdO/Al_2O_3, indicating the feasibility of its use in catalytic compositions.

Acknowledgement

The authors would like to thank the Center for Collective Use at the D.I. Mendeleev Russian Chemical Technology University for conducting research on the elemental composition of the samples.

The work was carried out as part of a state assignment from the Ministry of Science and Higher Education of the Russian Federation (FSSM-2023-0004 "Scientific foundations of transition metal-based catalysis systems for promising redox reactions of selective conversion of hydrocarbons and oxygen-containing organic substrates").

References

1. Direct Reduction Iron: Trends and Prospects. *Metallurgical Bulletin (Information and Analytical Journal)*. URL: https://www.metalbulletin.ru/a/199?ysclid=m7ls32q7hu658567728 (Access Date: 16.07.2025).

2. Lokteva E. S. Methods of Implementing the Processes of "Green" Chemistry. Moscow: Izdatelstvo Triumf, 2021. 270 p.

3. Technological Gorenje: a Collective Monograph. Eds. by Aldoshin S. M., Alymov M. I. Moscow: Russian Academy of Sciences, 2018. 612 p.

4. He L., Fan Y., Bellettre J., Yue J., Luo L. A Review on Catalytic Methane Combustion at Low Temperatures: Catalysis, Mechanisms, Reaction Conditions and Reactor Designs. *Renewable and Sustainable Energy Reviews*. 2020. Vol. 119. 109589.

5. Liberman E. Y., Simakina E. A., Izotova A. O., Kon'kova T. V., Grunsky V. N., Moiseev I. A. Synthesis and Activity of Nanodispersed $SNO_2 - CeO_2$ Catalyst in the Oxidation Reactions of Carbon Monoxide and Methane. *Kinetics and Catalysis*. 2021. Vol. 62, Iss. 1. pp. 155–159.

6. Toscani L. M., Curyk P. A., Zimicz M. G., Halac E. B., Saleta M. E, Lamas D. G., Larrondo S. A. Methane Catalytic Combustion Over $CeO_2 - ZrO_2 - Sc_2O_3$ Mixed Oxides. *Applied Catalysis A: General*. 2019. Vol. 587. 117235.

7. Chen S., Li S., You R., Guo Z., Wang F., Li G., Yuan W., Zhu B., Gao Y., Zhang Z., Yang H., Wang Y. Elucidation of Active Sites for CH_4 Catalytic Oxidation over Pd/CeO_2 Via Tailoring Metal–Support Interactions. *ACS Catalysis*. 2021. Vol. 11, Iss. 9. pp. 5666–5677.

8. Ivanova A. S. Physicochemical and Catalytic Properties of Systems Based on CeO_2. *Kinetics and Catalysis*. 2009. Vol. 50, Iss. 6. pp. 797–815.

9. Ivanov V. K., Shcherbakov A. B., Baranchikov A. E., Kozik V. V. Nanocrystalline Cerium Dioxide: Properties, Preparation, Application. Tomsk: Izdatelstvo Tomskogo Universiteta. 2013. 284 p.

10. Kuznetsova T. G., Sadykov V. A. Specific Features of the Defect Structure of Metastable Nanodisperse Ceria, Zirconia, and Related Materials. *Kinetics and Catalysis*. 2008. Vol. 49, Iss. 6. pp. 840–858.

11. Boronin A. I., Slavinskaya E. M., Danilova I. G., Gulyaev R. V., Amosov Yu. I., Kuznetsov P. A., Polukhina I. A., Koscheev S. V., Zaikovskii V. I., Noskov A. S. Investigation of Palladium Interaction with Cerium Oxide and Its State in Catalysts for Low Temperature CO Oxidation. *Catalysts Today*. 2009. Vol. 144, Iss. 3-4. pp. 201–211.

12. Gavrilova N. N., Nazarov V. N. Analysis of Porous Structure Based on Adsorption Data. Moscow: D. I. Mendeleev Russian Technical Technical University, 2015. 132 p.

13. Malyutin A.V., Liberman E. Yu., Mikhailichenko A. I., Avetisov I. Kh., Koshkin A. G., Konkova T. V. Catalytic Activity of Nanodisperse Solid Solutions $M_{0.1}Zr_{0.18}Ce_{0.72}O_2$, where M is a Rare Earth Metal in the Oxidation Reaction of Carbon Monoxide. *Kataliz v Promyshlennosti*. 2013. Iss. 3. pp. 54–59.

14. Simplício L. M. T., Brandão S. T., Domingos D., Bozon-Verduraz F., Sales E. A. Catalytic Combustion of Methane at High Temperatures: Cerium Effect on PdO/Al_2O_3 Catalysts. *Applied Catalysis A: General*. 2009. Vol. 360, Iss. 1. pp. 2–7.

NFM